Electron Transfer in Metal–Organic Molecules. A Time Resolved EXAFS and Optical Spectroscopy Study

ARTICLE · AUGUST 2011

DOI: 10.1002/jccs.201190001

3 AUTHORS, INCLUDING:

Jie Chen

University of Massachusetts Boston

378 PUBLICATIONS **5,477** CITATIONS

SEE PROFILE

Peter M Rentzepis

University of California, Irvine

378 PUBLICATIONS **9,485** CITATIONS

SEE PROFILE

Invited Paper

Electron Transfer in Metal-Organic Molecules. A Time Resolved EXAFS and Optical Spectroscopy Study

Jie Chen,[a]* Wei-Kan Chen[b] and Peter M. Rentzepis[b]*
[a]*Key Laboratory for Laser Plasmas (Ministry of Education) and Department of Physics, Shanghai Jiao Tong University, Shanghai 200240, P. R. China*
[b]*Department of Chemistry, University of California at Irvine, CA 92697, USA*

Received March 15, 2011; Accepted April 14, 2011; Published Online April 25, 2011

We have measured, by means of ultrafast x-ray absorption and optical spectroscopy, the M-O (M=Fe, Co) and Co-N metal to ligand bond length change as a function of time and the formation and decay of the excited states and intermediate species, after excitation with a 267 nm femtosecond pulse. These experimental data combined with DFT calculations allowed us to determine the mechanism of electron transfer operating in the redox reaction of two metal-ligand complexes, $[M(III)(C_2O_4)_3]^{3-}$ and $[Co(III)(NH_3)_6]^{3+}$. Based on the data we find that, even though both molecules are excited into their charge transfer band, the redox reaction of $[M(III)(C_2O_4)_3]^{3-}$ proceeds via intermolecular electron transfer while $[Co(III)(NH_3)_6]^{3+}$ electron transfer mechanism is intramolecular.

Keywords: Electron transfer; Ultrafast x-ray spectroscopy; Metal-organic molecule.

1. INTRODUCTION

Energy transfer by means of electrons[1,2] and protons[3-5] translocation from one atom or group to another within one molecule are commonly occurring processes in many areas of science. Electron transfer has been the subject of numerous theoretical and experimental studies, however very little information is available concerning the structure of the transient intermediate states and species evolved during the energy transfer process. Lately however, owing to the development of ultrashort hard x-ray and electron pulses by Synchrotrons and tabletop laser sources it has been possible to measure directly the transient structures of liquids and solids.[6-8]

To that effect intense characteristic emission lines as well as x-ray continua in the KeV range have been generated with subpicosecond duration through the interaction of very intense laser pulses with solid and liquid metal targets.[9] These pulses are used as probes to study transient structures with sub-Angstrom and subpicosecond resolution. One important advantage of the laser driven systems is the availability of optical pulses that can be precisely synchronized with the x-ray or electron beam pulses. Thus, the basic pump and probe experimental technique of optical ultrafast time resolved measurements could be implemented in the hard x-ray region. In these time resolved transient structure experiments presented here, an optical (pump) pulse is used to excite the sample while an accurately synchronized x-ray pulse (probe) is use to monitor the transient dynamics induced by the optical excitation pump pulse.

The two most commonly used x-ray absorption methods are XANES, X-ray Absorption Near Edge Structure and EXAFS, X-ray Absorption Fine Structure. The number of time resolved x-ray absorption studies published so far is rather limited, yet rather far reaching[10,11] and include: a gas phase ultrafast x-ray absorption experiment[12] of gaseous SF_6 and a time resolved XAS experiment, with 14 ns resolution, on the transient molecular structure in the liquid phase.[11,13] The chemical shift of photo excited aqueous $[Ru(bpy)_3]^{2+}$ was also measured with ~100 ps resolution[14] and later a similar tabletop x-ray system was used to study the structure of photo excited $[Fe(CN)_6]^{4-}$ in water with 30 ps resolution.[15] The X-ray absorption near-edge structure associated with photoinduced Fe(II) spin crossover reac-

* Corresponding author. E-mails: jiec@sjtu.edu.cn, pmrentze@uci.edu

tion has been studied using 70 ps, 7.1 KeV, tunable X-ray pulses derived from the Advanced Light Source.[16]

In this paper we present the experimental results obtained by the application of a tabletop femtosecond laser system for the generation of femtosecond hard x-ray pulses in the 6-22 KeV range and the utilization of these short x-ray pulses for the study of time resolved x-ray absorption phenomena, Fig. 1. Of the vast number of topics that can be investigated with these techniques we will restrict this paper to EXAFS studies aimed at the detection and measurement of the kinetics of the transient excited states and intermediates evolved during electron transfer. We describe here experiments that reveal the transient structure of ferrioxalate and cobalt ammine complexes in solution as electron transfer proceeds after excitation with an femtosecond optical pulse.

1.1. Time resolved x-ray diffraction

Time resolved x-ray diffraction has the potential to provide a complete, global picture of the structural changes of a process or reaction under study, without ambiguity in the interpretation and is especially appropriate for the investigation of crystalline materials. Time resolved x-ray diffraction experiments have been used for a decade to study transient structures in crystalline solids, especially metals with nanosecond and picosecond resolution[6] and recently, it has become possible to obtain data with subpicosecond resolution.[8]

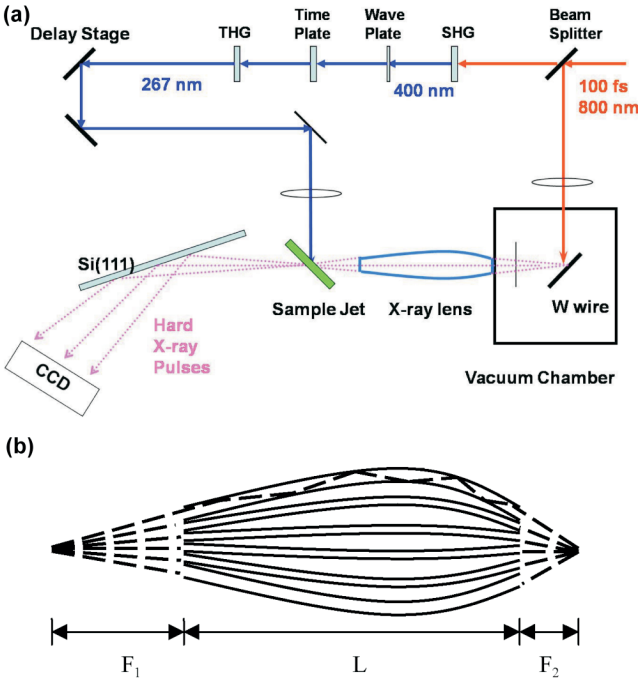

Fig. 1. (a) Dispersive ultrafast x-ray absorption spectrometer. (b) X-ray Polycapillary focusing lens.

The diffraction of monochromatic x-ray radiation from a crystal is governed by Bragg's law, therefore, even a very small change in the interatomic spacing of a crystal induces change in the Bragg condition that result in a measurable shift in the diffracted angle. The relation between the angle shift $\Delta\theta$ and the lattice spacing d is given by differentiation of Bragg's equation:

$$\Delta d/d = - \Delta\theta/\tan\theta$$

The angle shift, therefore, is a measure of the change in the spacing of the diffracting planes of the crystal. When laser radiation is absorbed by a very thin surface layer of a crystal, the temperature distribution and the associated stress in the bulk of the crystal will becomes nonuniform causing a distortion in lattice spacing. Such nonuniform lattice spacing distribution inside the crystal causes the diffraction signal to be scattered over a range of angles corresponding to the changes in lattice spacing. If the divergence of the incoming x-ray beam is sufficiently large to cover all of these angles, then the recorded signal will contain all of the information regarding lattice space changes obtained at different times. Experimentally, an entire rocking curve may be recorded in a single shot by illuminating the crystal with a divergent beam and using a large area CCD detector to record the reflected x-ray radiation over the entire scattered angle. The use of large area 2D CCD is rather mandatory because allows for recording, simultaneously, both signal and reference. The recorded x-ray signal is essentially the convolution of the crystal response to the probing x-ray pulse. The time resolution of these experiments depends not only on the duration of the pump and probe pulses and material response, but also on the propagation time of the fs pulses in the sample.

1.2. Time resolved x-ray absorption

X-ray diffraction is probably the best means for the study of structure of solids on the atomic level; however its application to liquid phase is very limited. Because many elementary reactions in chemistry and biology occur in the liquids phase, there is a need for efficient and accurate

methods that may be used to determine the structure of transients in solution. For liquid structure determination the x-ray absorption techniques[17] of XANES and EXAFS are preferred because they can measure very accurately local structure of molecules, including bond length changes, charge distribution, oxidation-reduction and coordination number of atoms and molecules. X-ray absorption has also the advantage of being very sensitive only to a particular atom therefore it determines the structure of the first few coordination layers away from the absorbing atom near the selected, absorbing, atom and is not affected by solvent impurities as long as they do not contain the absorbing atom. Many fundamental processes in nature, such as chemical reactions and phase transitions involve dynamic changes in their atomic arrangements, which take place on time-scales comparable to the oscillation periods of atoms and molecules. Therefore to understand the dynamics of chemical and biological process on such ultrafast time-scales, structural information with picosecond and femtosecond time resolution is necessary. Expanding EXAFS to the ps and fs time domain is rather important and quite challenging, because in EXAFS, the processes of electron ejection, backscattering and interference are extremely fast. For inner shell electrons with KeV energies these processes are essentially completed within a few femtoseconds. To display such data XANES and EXAFS should be able to take a real time, instantaneous picture of the atoms involved in an interaction[9,10] and display their transient bond distance and local structure. Owing to the improved techniques for the generation of ultrashort optical and hard x-ray pulses such experiments are now possible, because EXAFS broadband x-ray continua in a well-defined spectral region can be generated by tabletop laser induced plasma x-rays and synchrotron facilities. The structural information provided by EXAFS and XANES, is displayed in the form of modulation of the absorption spectrum located above the x-ray absorption edge.

2. EXPERIMENTAL

The experiments described in this paper were carried out on a tabletop Ti: Sapphire fs, laser system that generates both the optical fs pump pulses and the KeV x-ray continuum probe pulse. This laser system consists of a Spectra Physics Tsunami laser oscillator that emits 80 fs pulses at 82 MHz.[18] The 80 fs pulses seed a regenerative amplifier followed by a multi-pass power amplifier, which generates 100 fs, 100 mJ, 800 nm, 10 Hz pulses that are used to produce the fs x-ray pulses by focusing onto a 0.5 mm, or 0.25 mm diameter moving Cu, Mo or W wire located inside a vacuum chamber, Fig. 1a. The laser plasma induced x-ray radiation exits the chamber through a 0.25 mm thick Be window, covered by a rolling plastic tape that protect it from metal debris emitted by the evaporated metal. The upper limit of the x-ray pulse duration was measured by the thin crystal technique[18] and found to be 0.6 ps. The x-rays emitted by the W, Cu and Mo wires consist of both characteristic lines and continua were focused onto the sample by a polycapillary x-ray lens, Fig. 1b and their spectra were measured by means of an x-ray detector (2D CCD) and multichannel analyzer (XR-100CR and MCA8000A, Amptek, Inc.) as shown in Fig. 2. The energy range used was between 6 KeV and 22 KeV, with the low limit determined by the transmission of the chamber window, the plastic tape, air and the upper energy limit by the detector sensitivity. The spectra shown in Fig. 2 consist of both continuum radiation suitable for ultrafast x-ray absorption spectroscopy and characteristic line emission to be used for x-ray diffraction experiments. The spectra shown were recorded for 30 min and depict the raw count rate data without correction for x-ray chamber windows loss, air transmission and detector efficiency. The absolute photon yield of the x-ray source was estimated by correcting the measured values for the absorption along the x-rays path, by the

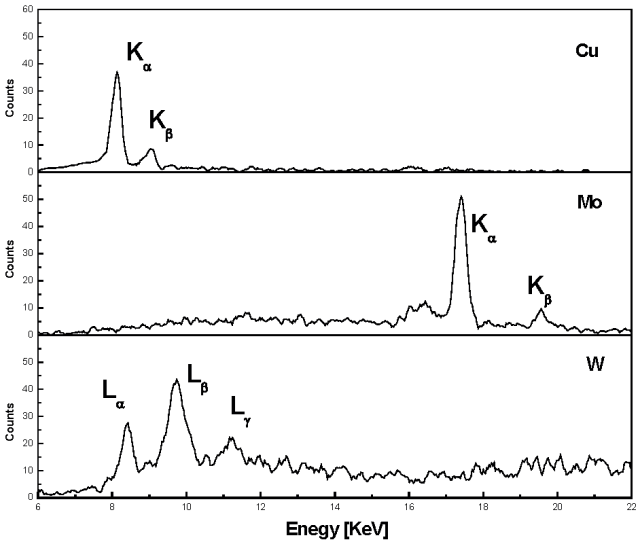

Fig. 2. X-ray spectra emitted by Cu, Mo and W wire.

plastic tape, Be windows and the air, as well the detector efficiency and assuming that the x-ray emission is isotropic in 4π steradians. As expected the fraction of bremsstrahlung increases with the Z number of the target. We have estimated that for 20 mJ laser pulse energy impinging on a copper wire target, 46% of the x-ray photons transmitted through the x-ray chamber belong to the CuKa characteristic line. The energy-dispersive setup (Amptek) allows for the entire spectrum to be recorded simultaneously. This is rather mandatory for measurements that utilize x-rays generated by high intensity laser plasma x-ray sources because the shot to shot fluctuations of the x-ray flux can be very high and affect adversely the entire spectrum.

2.1. Experimental System

The time resolved femtosecond x-ray absorption system used to detect and determine the structure and kinetics of transient's states and intermediates formed during the redox reaction of Fe(III) and Co(III) complexes is shown in Fig. 1. The sample was excited by a 100 fs, 400 nm or 267 nm laser pulse and probed by a 600 fs x-ray continuum pulse whose energy was located 1000 eV above the K absorption edge of the metal. Our EXAFS experimental system incorporates a dispersive spectrometer,[19] which allows for the entire XAS spectrum to be recorded simultaneously, thus decreasing the error caused by the shot to shot fluctuation in intensity of either beam. The output of the x-ray source was focused by a polycapillary x-ray lens Fig. 1b into ~ 0.120 mm diameter spot on the sample which flowed in the form of a 0.100 mm thick and 2 mm wide liquid jet. The probe, x-ray beam overlapped the UV beam at 90° and the jet at 45°. The sample solution was excited by 100 fs, 400 nm or 267 nm pulses. The light intensity impinging on the sample was 3×10^{12} W/cm^2, the probe x-ray pulse was dispersed by a 10 cm diameter Si (111) crystal situated 120 mm from the jet sample beam, and the reflected x-ray radiation was imaged onto the CCD surface.

2.2. Materials and absorption spectra

Ammonium ferrioxalate $(NH_4)_3[Fe(III)(ox)_3].3H_2O$, where ox = $C_2O_4^{2-}$ was purchased from Alfa Aesar and used without further purification. $(NH_4)_3[Co(III)(ox)_3]$ was prepared according to the procedure described in the reference[20] and purified repeatedly until its spectrum in water remained unchanged and all observable impurities were removed. The percentage of oxalate group in cobaltoxalate was analyzed and found to be 59.6 ± 1.3, which in agreement with the theoretical value 60.2. The absorption spectra, Fig. 3, show that ferrioxalate has two absorption bands with maxima at 210 nm ($\varepsilon = 1.2 \times 10^4$ cm^{-1}M^{-1}) and 669 nm ($\varepsilon = 0.94$ cm^{-1}M^{-1}). The spectra and extinction coefficients of these bands are in agreement with the corresponding literature values.[21-23]

2.3. Photochemistry of metal oxalate

The photochemistry of Fe(III) and Co(III) complexes has been studied for several years.[24-27] Yet the mechanism for the formation and decay of the excited states and intermediate species has not been reported at least in the fs and ps time regime, even though the quantum yield for the photo redox reactions has been investigated in depth and is used for chemical actinometry.[28] The mechanism of this redox process has been studied by flash photolysis at various pH values and concentrations and both steady state and pulsed irradiation experiments suggest that the quantum yield for the formation of Fe(II) exceeds 1.0 at 250-400 nm. To justify such a quantum yield it is expected that the mechanism of the primary photo process would involve the generation of fragments that react with parent molecules to reduce the ferrioxalate. In addition, the steady state quantum yield and temperature dependent experimental data point to rather low activation energy for the reaction of the fragments with ferrioxalate. Based on these conditions, a possible mechanism that has been proposed[24] is:

$$[Fe(III)(C_2O_4)_3]^{3-} \xrightarrow{h\nu} [Fe(II)(C_2O_4)_2]^{2-} + C_2O_4^{\bullet -}/CO_2, CO_2^{\bullet -} \quad (1)$$

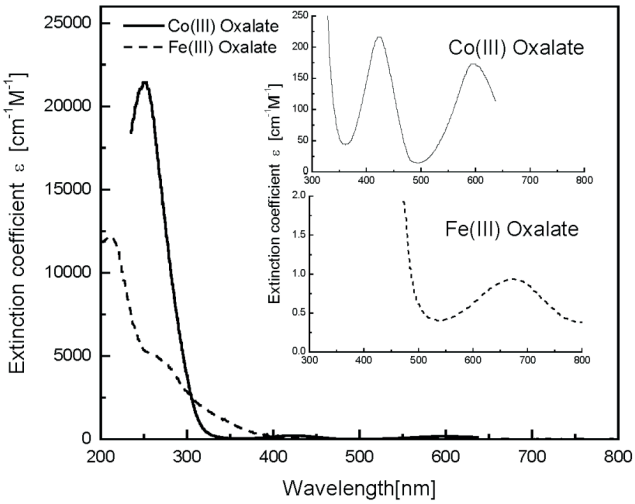

Fig. 3. Absorption spectra of cobaltoxalate and ferrioxalate in water. Insert: Enlarged absorption spectra from 300 nm to 800 nm.

$$[Fe(III)(C_2O_4)_3]^{3-} \xrightarrow{h\nu} [Fe(III)(C_2O_4)_2]^{-} + 2CO_2\bullet^{-} \quad (1a)$$

In H_2O solution:

$$[Fe(III)(C_2O_4)_3]^{3-} \xrightarrow[H_2O]{h\nu} [Fe(III)(C_2O_4)_2(H_2O)_2]^{-} + C_2O_4^{2-} \quad (2)$$

$$[Fe(III)(C_2O_4)_2(H_2O)_2]^{-} + C_2O_4^{2-} \rightarrow [Fe(III)(C_2O_4)_3]^{3-} \quad (3)$$

Several interesting ns to ms time resolved flash photolysis experiments have been reported which provide valuable insight into the ferrioxalate photoreaction.[29] Even at the rather slow ns/ms experimental resolutions, it is evident that the first order dependence of the Fe(III) complex decomposition to Fe(II) involves a Fe(III)Fe(II) electron transfer.[29] However, these experiments cannot distinguish between reaction 1 and 1a. This ambiguity is **very** important for the time resolved EXAFS experiments presented here because we are concerned only with the photoreaction transients formed during the first 25 ps.

We have extended the steady state and flash photolysis studies to the picosecond and femtosecond regime. The Fe(III) and Co(III) photoredox reaction experiments presented in this article were conducted in air at room temperature using 100 fs, 0.3 mJ, 267 nm pulses. The experimental system utilized was an optical ultrafast pump/probe absorption laser system composed of a Ti: Sapphire laser emitting 130 fs pulses at 800 nm. In addition, a 6 ns Nd: YAG laser was used for the ns to ms experiments. The pump pulse for the nanosecond experiments was the third harmonic, 355 nm of the Nd:YAG laser and the 400 nm SHG and 267 nm THG of the Ti:Sapphire for fs/ps experiments. The probe beam for the fs and ps experiments consisted of a broad optical continuum, of the same duration as the pump pulse, that covered the 300-600 nm spectral region and a high pressure xenon lamp for ns to ms experiments. The detector was either a fast photomultiplier coupled to an oscilloscope for nanosecond experiments or, a CCD coupled to a computer for the ps/fs experiments.

The femtosecond data, Fig. 4, show that an intermediate is formed at 430 nm, immediately after excitation, achieves its maximum absorption intensify after 2.6 ps and then remains constant for at least 610 ps. Using the nanosecond system we determined that the 430 nm band decays with a lifetime of ~ 4 ns. Based on these data, we propose the following mechanism:

$$[Fe(III)(C_2O_4)_3]^{3-} \xrightarrow[fs]{h\nu} [Fe(III)(C_2O_4)_3]^{3-*} \quad (5)$$

$$[Fe(III)(C_2O_4)_3]^{3-} \xrightarrow[\approx 1\,ps]{} [(C_2O_4)_2Fe(III)(\text{-}OC_2O_3)]^{3-} \rightarrow [Fe(III)(C_2O_4)_2]^{-} + 2CO_2\bullet^{-} \quad (6)$$

$$[Fe(III)(C_2O_4)_2]^{-} + CO_2\bullet^{-} \rightarrow [Fe(II)(C_2O_4)_2]^{2-} + CO_2 \quad (7)$$

$$[Fe(II)(C_2O_4)_2]^{2-} \xrightarrow{H_2O} [Fe(II)(C_2O_4)_2H_2O]^{2-} \rightarrow [Fe(II)(C_2O_4)_2(H_2O)_2]^{2-} \quad (8)$$

which agrees with the previous time resolved experimental data performed with longer time resolution. We have correlated the structure determined by the time resolved EXAFS data with the transient species evolved during the photochemical process, especially the transient structures evolved during the first 100 ps after excitation in order to arrive at the Fe(III) → Fe(II) electron transfer mechanism that we propose.

2.4. Solvated electron absorption spectra

A 500-800 nm transient absorption band with maximum at 720 nm, formed immediately after excitation with 266 and 267 nm pulses, Fig. 5, which is similar to the well known broad, structureless absorption band of the solvated electrons in water.[30,31] The decay lifetime of this absorption band is shown in Fig. 6 and its dependence on concentra-

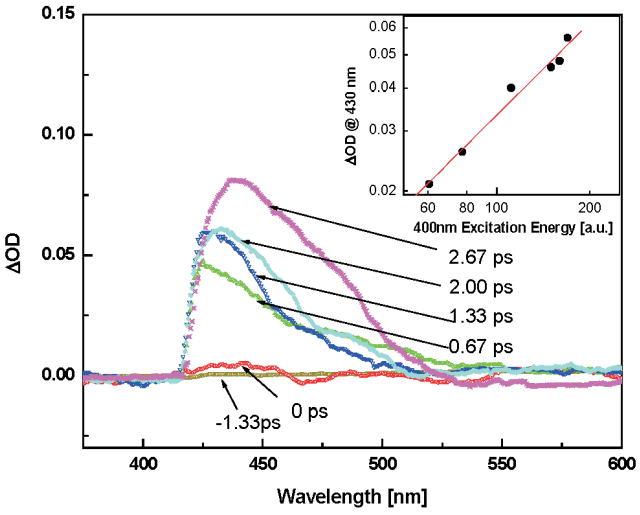

Fig. 4. Femtosecond transient absorption spectra of ferrioxalate in water excited by 400 nm pulses. Insert: the energy dependence of the transient optical density at 430 nm.

tion in Fig. 7. Also, its formation and decay kinetics are in agreement with the reported time resolved spectra and formation kinetics observed for solvated electrons.[30,31] Using the quantum yield of ferrocyanide which is reported to be about one,[32] the quantum yield for the photodetachment of an electron from ferrioxalate was estimated to be 0.05. The existence of solvated electrons in both Fe(III) and Co(III) complexes, after excitation, was confirmed by electron quenching experiments using 0.1-0.2 M KNO_3 as the electron quencher.[32,33]

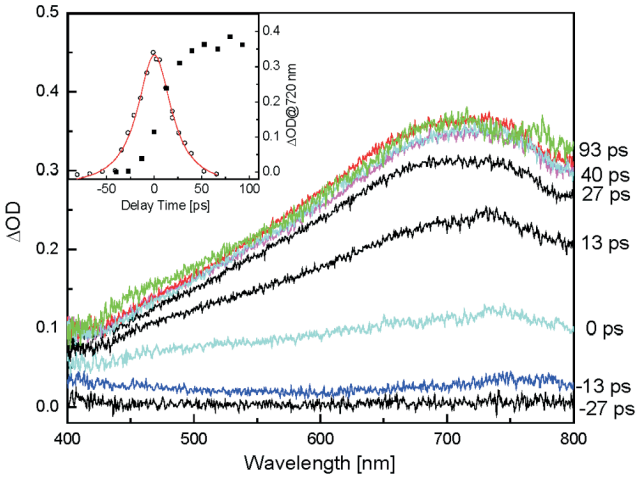

Fig. 5. Picosecond transient absorption spectra of 1.0 × 10^{-3} M cobaltoxalate in water using 266 nm excitation. Insert: transient kinetics at 720 nm (solid square points) and the 45 ps pulse width (open circle points fitted with solid line).

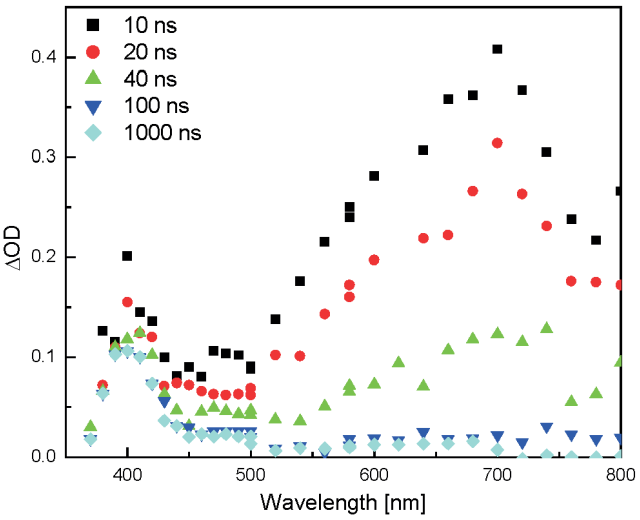

Fig. 6. Nanosecond transient absorption spectra of 2.3 × 10^{-3} M ferrioxalate in water (266 nm excitation).

2.5. Photoelectron detachment mechanism

Solvated electrons were generated by photoelectron detachment from the Fe(III)(ox) anion by excitation with 267 nm, 4.7 eV, pulses. Charge transfer to solvent (CTTS) theoretical and experimental studies have been performed[34] and also applied specifically to ferrocyanide and other charge transfer systems.[31,35] The ionization potentials for Co(III) and Fe(III) atom are reported to be I_p = 7.86 eV and I_p = 7.87 eV, respectively[36] and the photoelectric threshold has been determined to be ~3.2 eV for the hydrated electron in bulk water solution, which also corresponds to the solvation energy of the electron in water.[37] The difference of 4.66 eV between these two values is therefore the minimum energy needed to excite the M(III)(ox) molecule to the CTTS state. This suggests that one exciting 267 nm, 4.7 eV photon has sufficient energy to excite the ferrioxalate molecule to the metastable CTTS 4.66 eV state, and yield detached electrons that we observe in the form of solvated electron whose spectra and their formation and decay life times are shown in Figs. 5 and 6, respectively.

2.6. Time resolved EXAFS

We measured the Fe-O bond length of the parent Fe(III) oxalate molecule in solution using both a standard an x-ray diffraction system and also our time resolved EXAFS set-up without photoexcitation of the sample. We

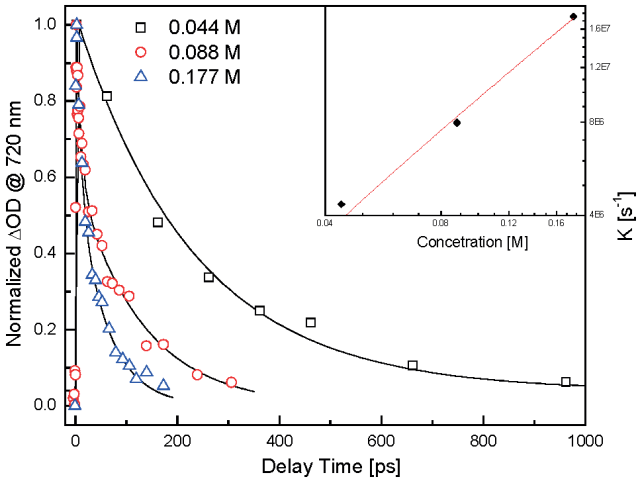

Fig. 7. Time resolved transient kinetics of Ferrioxalate in water at different concentrations after 266/267 nm excitation (square: 0.044 M, circle: 0.088 M and triangle: 0.177 M). The solid lines are exponential decay fits to the experimental data. Insert: the reaction rate constant at different concentration and the solid line is a linear fit to the experimental data.

find that the bond length values obtained from these experiments and the ones listed in the literature to be in good agreement with each other.

Then, we performed time resolved EXAFS experiments using the system presented schematically in Fig. 1, with excitation provided by a 267 nm or 400 nm, 100 fs optical pulse and using the 600 fs x-ray continuum pulse as probe. The pump pulse was absorbedly a 0.150 mm by 1.5 mm section of the flowing ferrioxalate solution and the same volume was intersected by the 0.6 ps x-ray probe pulse. The pump and probe pulses were made to overlap at the same time and place within the flowing liquid jet volume. The $(NH_4)_3Fe(III)(C_2O_4)_3$ sample was dissolved in water to a concentration of 1 g/mL of water which correspond to μx ~1. A volume of 100 mL of the sample was circulated through a metal jet that formed a 100 mm by 2 mm liquid column. We estimated that only 20% of the 150 mm volume was excited by each excitation pump pulse; therefore the amount of product formed was negligible compared to the 100 mL total volume.

To measure the structure of the intermediates evolved during the course of the photochemical reaction, EXAFS spectra were recorded at 2 ps time intervals between 20 ps before and 100 ps after excitation. Typical EXAFS spectra obtained from Fe(III) oxalate in q-space is shown in Figs. 8 and 10 after transformation to μx vs. E for –20 ps and +25ps in Fig. 9. Similar EXAFS spectra have been measured up to 100 ps delay time after excitation. The –20 ps spectrum is assigned to the $[Fe(III)(C_2O_4)_3]^{3-}$ parent molecule before excitation and the +25 ps EXAFS spectrum to a transient species that lives for 25 ps after excitation and subsequently decays to another intermediate, which in turn, decays, after several milliseconds, to the final Fe(II) product.

The μx vs. E spectra were transformed to |χ(R)| vs. R[Å] spectra, Fig. 10, that display the bond length for the first two coordination shells near the iron atom at –20 ps before excitation and +25 ps after excitation. From the |χ(R)| vs. R spectra, the Fe(III)–O distance was determined

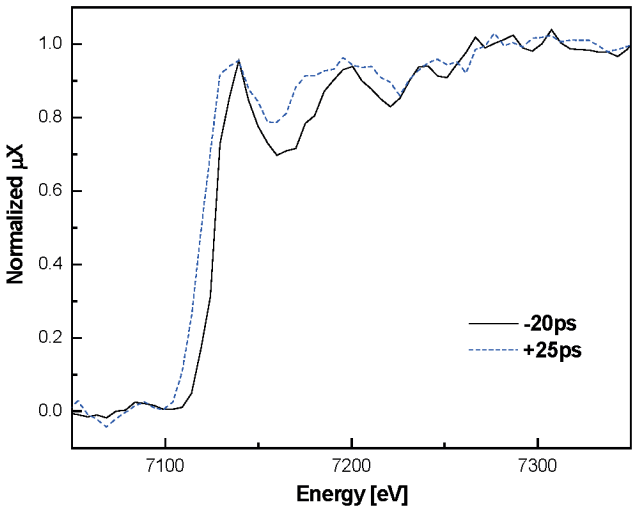

Fig. 9. Fe K-edge X-ray absorption spectra of ferrioxalate/water solution before (solid, -20 ps) and after (point, +25 ps) UV radiation.

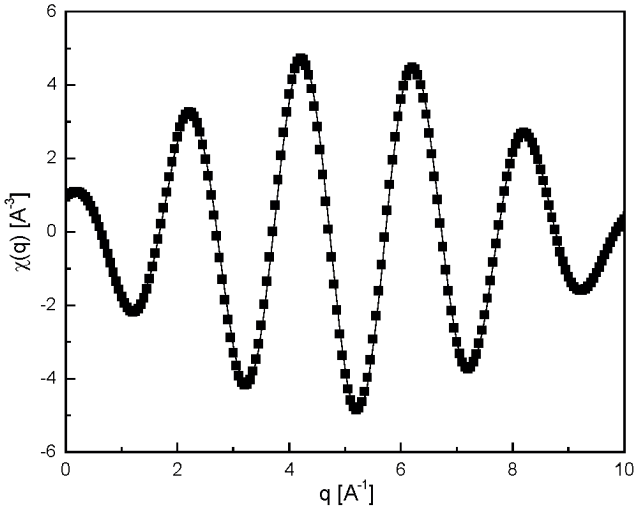

Fig. 8. EXAFS spectra in q-space of ferrioxalate/water solution by femtosecond system 20 ps before excitation (line) and a CW source (scatter).

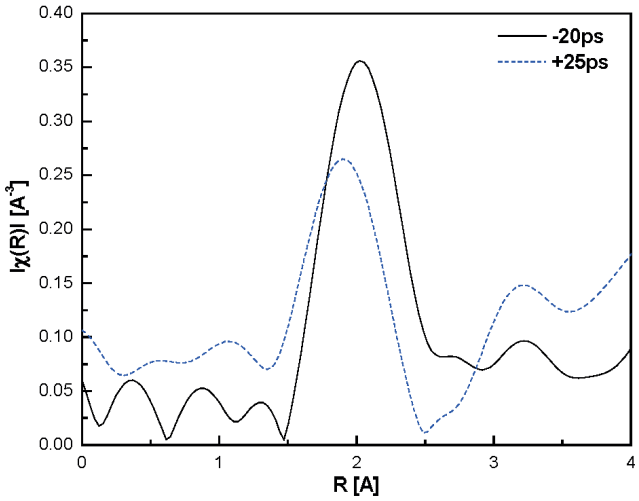

Fig. 10. Fe(III)ox EXAFS spectrum in R space of ferrioxalate/water solution before (solid, -20 ps) and after (point, +25 ps) UV radiation.

to be 2.02 Å for the parent molecule (–20ps) and 1.84 Å for the transient formed +25 ps after excitation. The values for the Fe(III)–O bond distance measured by the CW system was determined to be 1.98 Å that compares very favorably with the 2.00 Å value listed in the literature.[38] Both of these bond lengths are also in very good agreement with the 2.02 Å value obtained, at 20 ps before excitation. The Fe-O bond length at +25 ps after excitation was determined to be 1.84 Å by our fs-time resolved EXAFS system, which is shorter than that of the stable parent molecule. We assigned the +25 ps transient to $[Fe(III)(C_2O_4)_2]^-$ four coordinate transient species. The shorter Fe-O bond length maybe due to the bonding of the iron to four oxalate oxygen atoms instead of the six oxalate oxygen atoms that are bound to the non-excited parent $(NH_4)_3Fe(III)(C_2O_4)_3$ complex.

The time resolution of the experiments reported here is 2 ps. EXAFS experiments at 2 ps suggest that the excited state Fe-O bond length is longer than the bond length of the ground state. During the first 2 ps time after excitation while the parent molecule is in the excited state, the (C_2O_4) moiety is intact and has not been cleaved yet. However, during these first two picoseconds after excitation, electron transfer from $[Fe(III)(C_2O_4)_3]^{3-}$ to $Fe(II)(C_2O_4)_3]^{3-}$ may have taken place even before the first oxalate ligand is cleaved. Optical data suggest that during the first 4 ps after excitation dissociation involving an oxalate ligand takes place resulting in the formation of the $[(C_2O_4)_3Fe(III)\text{-}(\text{-}OC_2O_3)]^{3-}$ five coordinate intermediate. This molecule subsequently dissociates to the four coordinate transient $[Fe(III)(C_2O_4)_2]^-$ molecule that we measured to have a Fe-O bond length of 1.84 Å and persist with nanosecond lifetime and have assigned this intermediate species to the same transient that was observed at +25 ps after excitation. Time resolved optical experiments suggest that $[Fe(III)(C_2O_4)_2]^-$ will react with $CO_2^{\cdot-}$ radical by intermolecular electron transfer forming $[Fe(II)(C_2O_4)_2]^{2-}$ transient in nanosecond range. Time resolved optical experiments suggest that several ms after excitation, water is attached to the $[Fe(II)\text{-}(C_2O_4)_2]^{2-}$ molecule to form $[Fe(II)(C_2O_4)_2\text{-}(H_2O)_2]^{2-}$. Consequently the Fe atom becomes six coordinated and the Fe-O bond length increases to 2.16 Å. The crystalline $[Fe(II)(C_2O_4)_2\text{-}(H_2O)_2]^{2-}$ has been investigated by x-ray diffraction and the Fe-O (oxalate) bond distance has been determined to be 2.11-2.20 Å.[39] The Fe-O bond lengths at times after excitation and their assignment to transients are listed in Table 1.

Based on the time resolved optical and EXAFS data presented here and the supporting quantum mechanical DFT and H-F calculations we propose that dissociation precedes electron transfer and the photo-induced redox reaction mechanism of Fe(III)ox to Fe(II)ox is described by reactions 5-8. Similar results had been observed for Co(III)ox.[40] This mechanism is supported by:

a. The Fe-O bond distance of the transient intermediate being shorter than the Fe(II)-O bond distance strongly indicates that this intermediate is an Fe(III) intermediates and not Fe(II).

Table 1. Fe–O bond length at various delay times before and after excitation obtained by time resolved EXAFS and quantum chemistry calculations using Gaussian 03 program

Delay Time	Assignment	Ligand	Exp. R (Å)	Cal. R (Å)	
				UHF	DFT
-20 ps	$Fe(III)(C_2O_4)_3^{3-}$	C_2O_4	2.02	2.04	2.01
1-2 ps	$[Fe(C_2O_4)_3^{3-}]^*$	C_2O_4	2.16	N/A	N/A
4 ps	$[C_2O_3O\text{-}Fe(III)(C_2O_4)_2]^{3-}$	C_2O_3O C_2O_4	1.93-2.09	1.87 2.01	1.87 2.02
9-115 ps	$Fe(III)(C_2O_4)_2^-$ Tetrahedral-like	C_2O_4	1.87-1.93	1.90	1.90
110 ns-2 ms	$Fe(II)(C_2O_4)_3^{4-}$	C_2O_4	N/A	N/A	N/A
	$Fe(II)(C_2O_4)_2^{2-}$ Tetrahedral-like			2.04	2.01
Final product	$[Fe(II)(C_2O_4)_2(H_2O)_2]^{2-}$	H_2O C_2O_4	2.11 2.20	2.15 2.16	N/A N/A

b. The energy of the exciting photon is sufficient to break both the Fe-O and C-C bonds of the ferrioxalate molecule to form $CO_2^{\cdot-}$ radicals that subsequently react with and reduce the parent molecule via an intermolecular electron transfer mechanism.

c. The observation of the $CO_2^{\cdot-}$ radical is a further confirmation of the intermolecular mechanism.

3. REDOX REACTION MECHANISM OF $[Co(III)(NH_3)_6]Ac_3$

We performed similar optical, XAS experiments and DFT calculations to the ones described for $M(ox)_3$ complex, using $[Co(III)(NH_3)_6]^{3+}$ complex. The UV/VIS absorption spectrum of $[Co(III)(NH_3)_6]Ac_3$ is composed of three well-separated absorption band bands: a charge transfer band, CT, with maximum at ~250 nm and two ligand-field bands with maxima at ~345 nm and 470 nm, respectively, Fig. 11. Immediately after excitation with a 267 nm fs pulse, into the CT band, we detected the formation of a transient that consisted of a broad, structureless absorption band, extending from ~480 nm to 820 nm and reached its maximum intensity at ~720 nm in less than 2 ps after excitation, Fig. 12. All characteristic and kinetics of this absorption band area very similar to the well-known absorption band of solvated electrons in water. We found that this solvated electron absorption band decays with two reaction rates: **a)** a cage germinate recombination reaction which occurs in the 10^{11} s^{-1} range and **b)** an out of cage diffusion controlled, slow reaction, which is practically identical to the intermolecular electron transfer reaction corresponding to reactions 10 and 11, that is shown in Fig. 6. The quantum yield for the generation of solvated electrons was determined to be 0.05, which is essentially an order of magnitude smaller than the quantum yield of 0.5 for the electron transfer Co(II) formation process. Therefore the photoelectron detachment reaction is considered to be a minor side reaction that does not play an important role in the mechanism of the Co(III) to Co(II) redox reaction.

$$[Co(III)(NH_3)_6]^{3+} \xrightarrow{h\nu} [Co(NH_3)_6]^{4+} + e_{aq}^{-} \quad (9)$$

$$[Co(NH_3)_6]^{4+} + e_{aq}^{-} \rightarrow [Co(III)(NH_3)_6]^{3+} \text{ (in cage recombination)} \quad (10)$$

$$[Co(III)(NH_3)_6]^{3+} + e_{aq}^{-} \rightarrow [Co(II)(NH_3)_6]^{2+} \quad (11)$$

The dominant reaction after photoexcitation is intramolecular transfer of one electron from the ammonium ligand to cobalt and consequently the change of oxidation state of cobalt from +3 to +2. There are various experimental methods that allow one to measure directly the redox process, such as time resolved optical transient absorption spectroscopy, which can distinguish between the Co(III) and Co(II) complexes. However, for this molecule the very intense, broad solvated electron absorption band that is formed immediately after excitation and persists for several ns at which time the redox reaction is completed masks

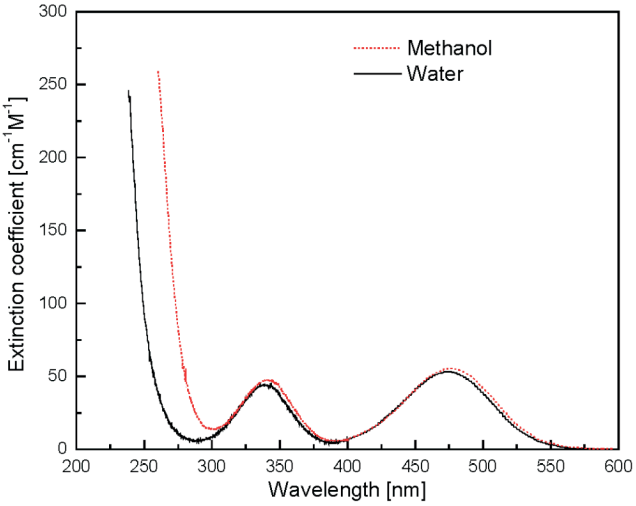

Fig. 11. Absorption spectra of $[Co(III)(NH_3)_6]Ac_3$ in water (solid line) and methanol (dotted line) solution.

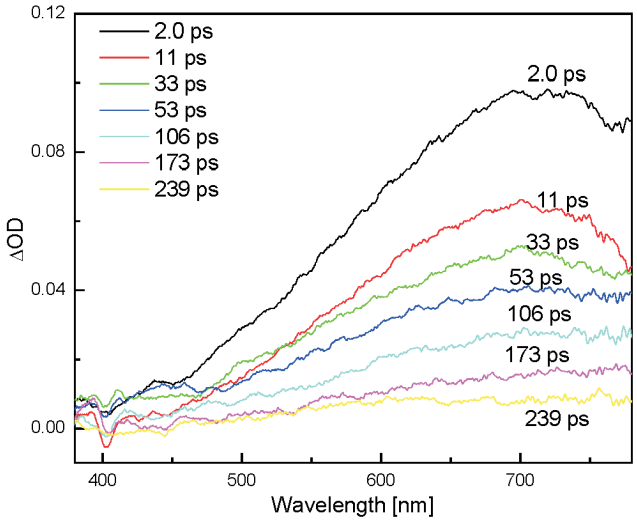

Fig. 12. Picosecond time resolved transient absorption spectra of 0.088 M hexamminecobalt(III) acetate in water after 267 nm excitation from 2.0 ps to 239 ps.

the relevant data. No other transients were detected that decayed with nanosecond or longer rates. Using our ultrafast time resolved EXAFS system we were able to determine the redox mechanism by measuring the Co-N bond length changes as a function of time.

3.1. $[Co(NH_3)_6]Ac_3$ ultrafast EXAFS studies

The picosecond time resolved EXAFS experiments were performed using the same tabletop pulsed laser and ultrashort x-ray system and procedure used for the Fe(III) ox studies. The concentration of the Co(III) complex sample, that flowed through the same jet was 1 g Co(III) complex/1 mL water corresponding to μx ~1.0 for 7.7 KeV. The |χ(R)| vs. R spectra, Fig. 13 display the Co-N bond length bond distance of the first coordination shell at 0 and 2 ps after excitation. The bond length difference between Co(III)-N and Co(II)-N is 0.18-0.21 Å, suggesting that there is 10% change in bond lengths between Co(III)-N and Co(II)-N. These data and the quantum chemistry theoretical calculations of the ground state structure of both the Co(III) and Co(II) complexes and transient structures which agree very well with the time resolved EXAFS experimental Co-N bond data and serve as the basis for the proposed mechanism of the photo induced Co(III) to Co(II) complex redox reaction.

Full geometry optimizations were performed for the Co(III) complex, also using the ground state and local spin density approximation. The results of ground state structure calculations and the assigned transient structures of the cobalt hexamine complexes are summarized in Table 2. The calculation of low spin, S = 0 $[Co(III)(NH_3)_6]^{3+}$ ion and high spin, S = 3/2, $[Co(II)(NH_3)_6]^{2+}$ ion structure was started using the published crystal structure without further symmetry restrictions. We determined by the LSDA method, that the $[Co(III)(NH_3)_6]^{3+}$ complex had S_6 symmetry giving a value of 1.95 Å for the Co(III)-N bond length which agrees with the 1.93 Å experimental value and with the 1.936-1.965 Å literature values[41,42] and the 1.93(2) Å value measured by our time resolved EXAFS experiments for the parent molecule before excitation. These Co-N bond lengths were further confirmed by steady state EXAFS experiments using a conventional x-ray tube system. These experiments yielded a 1.93(5) Å value for Co(III)-N bond length, which is also very close to the literature, and our time resolved EXAFS values for -10 ps before excitation.

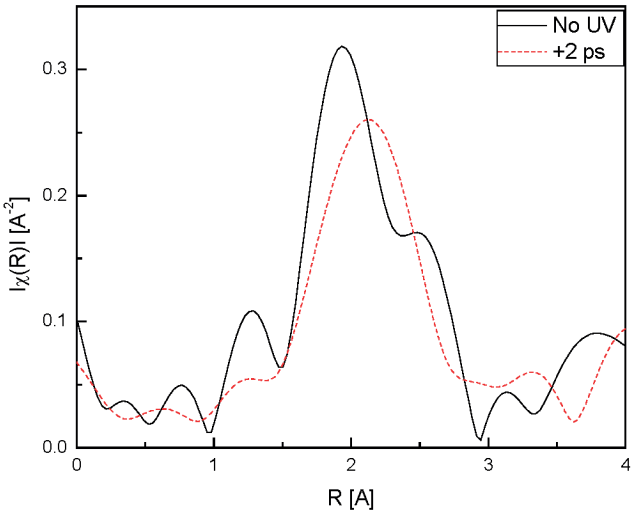

Fig. 13. R-space EXAFS spectra recorded for hexamminecobalt(III) complex (without excitation, solid) and hexamminecobalt(II) complex (+2 pts after excitation, dot).

Subsequently, we measured the Co-N bond length changes as a function of time after photo excitation with 0.2 mJ, 100 fs, 267 nm pulses. At 0 ps when both optical pulse and x-ray pulse overlap with each other, the Co-N bond length was determined experimentally, to be 1.96(3) Å which agrees well with the Co-N bond length we measured without UV excitation. We assigned the 0 ps transient to an excited state of the $[Co(III)(NH_3)_6]^{3+}$ complex with a structure very similar to the parent molecule. At 2 ps after excitation the |χ(R)| vs. R[Å] spectra, Fig. 13 show that the Co-N bond distance becomes 2.13(2) Å or 0.20 Å longer than that of the Co(III) parent molecule, Fig. 12. At 2 ps the Co-N bond length was measured to be 2.11 (6) Å and at 100 ps was 2.11(7) Å. Therefore, we concluded that the Co-N bond length remains constant, within experimental error, between 2 ps and 100 ps.

The experimental bond length difference between the Co(III) complex and Co(II) complexes is 0.19 Å, which is within the 0.18-0.21 Å range listed in the literature and the B3LYP/6-31G calculated range of 0.21-0.23 Å. These data provide additional strong support for the accuracy of the time resolved EXAFS experimental data. All data experimental EXAFS and theoretical calculation indicate that within 2 ps, after 267 nm irradiation of the Co(III) complex, an electron is transferred from the ligand to the metal forming Co(II)-N by an intramolecular electron transfer mechanism.

Table 2. Co-N bond length obtained by time resolved EXAFS and quantum chemistry calculations at various delay time before and after 267 nm excitation

Assignment	$[Co(III)(NH_3)_6]^{3+}$	$[Co(II)(NH_3)_6]^{2+}$	$\Delta d_{Co(II)-Co(III)}$
Exp. R (Å)	1.93	2.12	0.19
Cal. R (Å) LSDA	1.950	N/A	N/A
Cal. R (Å) B3LYP	2.030	2.237-2.256	0.21-0.23
Literature R (Å)	1.936(15)[39,43]	2.114(9)[39,43]	0.18[39]
Literature R (Å)	1.965(1) [41,44]	2.170(2)[44]	0.205(3)[44]

3.2. Comparison of the $[Co(III)(NH_3)_6]^{3+}$ and $[Co(III)(C_2O_4)_3]^{3+}$ redox reaction mechanisms

In Fig. 14 the metal-ligand bond distance changes of the Co-N bond in $[Co(III)(NH_3)_6]^{3+}$ and the Co-O bond in $[Co(III)(C_2O_4)_3]^{3-}$ are plotted vs. time, after 267 nm excitation. The Co-O bond length of the parent Co(III) complex has a value of 1.90 Å, that increases to 1.98 Å in less than 2 ps is assigned to an excited state. It is followed by a decrease to 1.93 Å after 2 ps, and then a further decrease to 1.78 Å after 4 ps, assigned to a transient after dissociation of Co(III)-O bonds. At times longer than 4 ps the Co-O bond length increased to 1.81 Å and remained as such for at least 142 ps which is assigned to a Co(III) transient. We have not detected a structure, which we could assign to Fe(II) product. However, based on these bond distance changes of the Fe(III) oxalate complex we propose that the redox reaction proceeds through a photodissociative reaction followed by inter-molecular electron transfer, before significant intramolecular electron transfer could take place. In contrast, the Co(III) amine complex photoredox reaction yields the Co(II) product within 2 ps, which strongly suggests that Co(II) amine redox product is formed immediately after irradiation by means of an intramolecular electron transfer mechanism. These two examples show that although both redox reactions are initiated by excitation in the CT band and yield the Co(II) product with the same 0.5 quantum, yet their photoredox reaction mechanisms are completely different. The difference in the mechanism between these two molecule and probably others is due to the competition between the rates of dissociation and intramolecular electron transfer. A major factor, which determines which mechanism will dominate, depends on the efficiency rate, that the ligand group (the electron donor) aligns at the proper orientation with the central metal (the electron acceptor). In the case of the Co(III) amine complex, each amine ligand can rotate freely, independent of other amine groups. This relative freedom allows for fast orientation that favors intramolecular ET and the immediate 2 ps, formation of Co(II) amine complex. However, for the M(III) (M=Fe, Co) oxalate complex, to transfer an electron from the oxalate to the M(III), in-plane or out-of-plane nuclear motion is probably necessary for proper ligand and metal alignment, this probably leads to the dissociation of the metal oxalate complex during the alignment process and consequently intermolecular ET becomes the operating mechanism. The steric effect proposed here, may be only one factor that influences the course of the photoredox reaction.

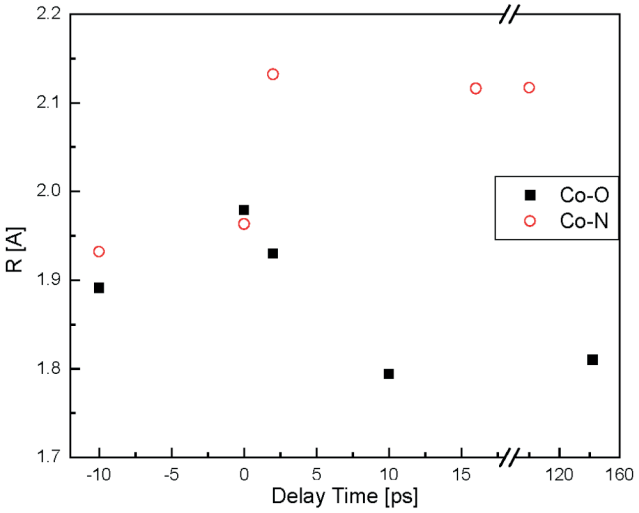

Fig. 14. Metal-ligand bond distance changes as a function of delay time: 1. Co-N bond in $[Co(III)(NH_3)_6]^{3+}$, circle; 2. Co-O bond in $[Co(III)(C_2O_4)_3]^{3+}$, square.

Based on our optical spectroscopic and time resolved EXAFS structural data and DFT calculations presented for hexamminecobalt(III) acetate complexes, after irradiation with 267 nm fs pulses, we have concluded that the primary photoredox reaction proceeds via intramolecular electron transfer from the ligand to metal, with solvated electron generation as a side reaction.

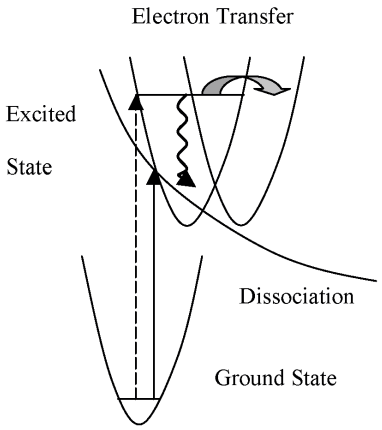

Fig. 15. Schematic diagram of intramolecular electron transfer and intermolecular electron transfer via dissociation mechanism of M(III) complex (L-ligand).

4. CONCLUSION

Ultrafast optical and x-ray spectroscopic data and supporting theoretical DFT and U-F calculations we have shown that the photoredox reaction of M(III)ox is controlled by an intermolecular mechanism, while the Co(III) amine follows an intramolecular electron transfer redox reaction. Even though both the $[Co(III)(NH_3)_6]^{3+}$ and $[M(III)-(C_2O_4)_3]^{3-}$ molecules were excited by the same intensity 267 nm pulses in their CT band. Therefore one cannot, priory, assign the mechanism of the redox reaction, based only on excitation into the CT band. The redox reaction path for these two mechanisms is displayed, schematically, in Fig. 15.

REFERENCES

1. Gray, H. B.; Malmstrom, B. G. *Comment Inorg. Chem.* **1983**, *2*, 203-209.
2. *Advances in Electron Transfer Chemistry*; Mariano, P. S., Ed.; JAI Press: Stanford, CT, 1999; Vol. 6.
3. *Proton Transfer*; Bamford, C. H.; Tipper, C. H. F., Eds.; Elsevier: Oxford, 1977; Vol. 17.
4. Kondo, M.; Heisler, I. A.; Stoner-Ma, D.; Tonge, P. J.; Meech, S. R. *J. Am. Chem. Soc.* **2010**, 132(*5*), 1452-1453.
5. Turro, C.; Bossmann, S. H.; Jenkins, Y.; Barton, J. K.; Turro, N. J. *J. Am. Chem. Soc.* **1995**, *117*, 9026-9032.
6. *Time Resolved Diffraction*; Helliwell, J. R.; Rentzepis, P. M., Eds.; Oxford University Press: Oxford, 1997.
7. Pfeifer, T.; Spielmann, C.; Gerber, G. *Rep. Prog. Phys.* **2006**, *69*, 443-505.
8. Rousse, A.; Rischel, C.; Gauthier, J. C. *Rev. Mod. Phys.* **2001**, *73*, 17-31.
9. Feurer, T.; Morak, A.; Uschmann, I.; Ziener, C.; Schwoerer, H.; Forster, E.; Sauerbrey, R. *Appl. Phys. B* **2001**, *72*, 15-20.
10. Bressler, C.; Chergui, M. *Chem. Rev.* **2004**, *104*, 1781-1812.
11. Chen, L. X. *Annu. Rev. Phys. Chem.* **2005**, *56*, 221-254.
12. Raksi, F.; Wilson, K. R.; Jiang, Z. M.; Ikhlef, A.; Cote, C. Y.; Kieffer, J. C. *J. Chem. Phys.* **1996**, *104*, 6066-6069.
13. Chen, L. X.; Jager, W. J. H.; Jennings, G.; Gosztola, D. J.; Munkholm, A.; Hessler, J. P. *Science* **2001**, *292*, 262-264.
14. Saes, M.; Bressler, C.; Abela, R.; Grolimund, D.; Johnson, S. L.; Heimann, P. A.; Chergui, M. *Phys. Rev. Lett.* **2003**, *90*, 047403.
15. Lee, T.; Jiang, Y.; Rose-Petruck, C. G.; Benesch, F. *J. Chem. Phys.* **2005**, *122*, 084506.
16. Khalil, M.; Marcus, M. A.; Smeigh, A. L.; McCusker, J. K.; Chong, H. H. W.; Schoenlein, R. W. *J. Phys. Chem. A* **2006**, *110*, 38-44.
17. Agarval, K. *X-Ray Spectroscopy*; Springer: New York, 1991.
18. Tomov, I. V.; Chen, J.; Ding, X.; Rentzepis, P. M. *Chem. Phys. Lett.* **2004**, *389*, 363-366.
19. Oulianov, D. A.; Tomov, I. V.; Lin, S. H.; Rentzepis, P. M. *J. Chin. Chem. Soc.* **2001**, *48*, 127-132.
20. Palmer, W. G. *Experimental Inorganic Chemistry*; University Press: Cambridge, 1970.
21. Balzani, V.; Carassiti, V. *Photochemistry of Coordination Compounds*; Academic Press Inc.: New York, 1970.
22. Jorgensen, C. K. *Adv. Chem. Phys.* **1963**, *5*, 33-146.
23. Copestake, T. B.; Uri, N. *Proc. Roy. Soc. London, Math. Phys. Sci.* **1955**, *228*, 252-263.
24. Cooper, G. D.; DeGraff, B. A. *J. Phys. Chem.* **1971**, *75*, 2897-2902.
25. Allmand, A. J.; Webb, W. W. *J. Chem. Soc.* **1929**, 1518-1531.
26. Livingston, R. *J. Phys. Chem.* **1940**, *44*, 601.
27. Parker, C. A. *Proc. Roy. Soc. London, Ser. A.* **1953**, *220*, 104-116.
28. Hatchard, C. G.; Parker, C. A. *Proc. Roy. Soc., Ser. A* **1956**, *235*, 518-536.
29. Horne, R. A. *J. Phys. Chem.* **1960**, *64*, 1512-1517.
30. Baxendale, J. H.; Capellos, C.; Land, E. J.; Keene, J. P.; Ebert, M.; Swallow, A. J.; Davies, J. V.; Francis, J. M.; Gilbert, C. W.; Fielden, E. M.; Nosworthy, J. M. *Nature* **1964**, *201*, 468-470.
31. Pommeret, S.; Naskrecki, R.; van der Meulen, P.; Menard, M.; Vigneron, G.; Gustavsson, T. *Chem. Phys. Lett.* **1998**, *288*, 833-840.
32. Wiesenfeld, J. M.; Ippen, E. P. *Chem. Phys. Lett.* **1980**, *73*, 47-50.
33. Jonah, C. D.; Miller, J. R.; Hart, E. J.; Matheson, M. S. *J. Phys. Chem.* **1975**, *79*, 2705-2711.
34. Blandamer, M. J.; Fox, M. F. *Chem. Rev.* **1970**, *70*(1), 59-93.

35. Sauer, M. C.; Crowell, R. A.; Shkrob, I. A. *J. Phys. Chem. A* **2004**, *108*, 5490-5502.
36. Schildcrout, S. M.; Pearson, R. G.; Stafford, F. E. *J. Am. Chem. Soc.* **1968**, *90*, 4006.
37. Coe, J. V.; Lee, G. H.; Eaton, J. G.; Arnold, S. T.; Sarkas, H. W.; Bowen, K. H.; Ludewigt, C.; Haberland, H.; Worsnop, D. R. *J. Chem. Phys.* **1990**, *92*, 3980-3982.
38. Merrachi, E. H.; Mentzen, B. F.; Chassagneus, F.; Bouix, J. *Rev. Chim. Miner.* **1987**, *24*, 56-67.
39. Kime, N. E.; Ibers, J. A. *Acta Crystallogr., Sect. B: Struct. Sci.* **1969**, *B25*, 168-169.
40. Chen, J.; Zhang, H.; Tomov, I. V.; Ding, X.; Rentzepis, P. M. *Proc. Nat. Acad. Sci. U.S.A.* **2008**, *105*, 15235-15240.
41. Beattie, J. K.; Moore, C. J. *Inorg. Chem.* **1982**, *21*, 1292-1295.
42. Kruger, G. J.; Reynhardt, E. C. *Acta Crystallogr., Sect. B: Struct. Sci.* **1978**, *34*, 915-917.
43. Barnet, M. T.; Craven, B. M.; Freeman, H. C. *Chem. Commun.* **1966**, 307-308.
44. Newman, J. M.; Binns, M.; Hambley, T. W.; Freeman, H. C. *Inorg. Chem.* **1991**, *30*, 3499-3502.